VALIDATION PLAN FOR COMPOUND SPLIT, VARIABLE ROTOR SPEED DRIVETRAIN

Christopher Gross, Advanced Drivetrain Technologies, Vienna, Austria
Andreas Juen, Advanced Drivetrain Technologies, Vienna, Austria
Lorenz Braumann, Advanced Drivetrain Technologies, Vienna, Austria
Hanns Amri, Advanced Drivetrain Technologies, Vienna, Austria

Abstract

This publication presents a validation plan for a transmission variable compound split drivetrain which is used for in flight rotor speed variation of rotorcraft. The validation is performed on a smaller-scale demonstrator at 300kW instead of 1MW. Scaling of the drivetrain can reduce the costs and increase the safety of the tests. To enable the extrapolation of the test results to the full-size application a scaling method for the boundary conditions and the mechanical properties was developed. The scaling method was validated using gear calculation software and modal analyses. The deviation of the gear safety factors is less than 5% while the modal analyses and shaft calculations show that the scaling method predicts a similar behaviour. Based on this scaling method a demonstrator was designed to reflect accurate behaviour of rotor speed variation mechanisms. A test plan to prove the functionality and safety of the Vari-Speed Drivetrain with the scaled demonstrator was developed. The research is part of the international research project VARI-SPEED-II which aims to enable main rotor speed variation for rotorcraft.

1. NOTATION[1]

Symbols:

L	Ratio of Lengths, -
n_{in}	Input speed CS (Turbine), rpm
n_{out_MP1}	Output speed CS at MP1, rpm
n_{out_MP2}	Output speed CS at MP2, rpm
P_{in}	Power at the input shaft (Turbine), kW
P_{TSE}	Power at the Turboshaft engine, kW
$P_{var,max}$	Max. Power of the variator machine, kW
R	Spread, -
T_{in}	Input moment CS (Turbine), Nm
T_{out_MP1}	Output moment CS at MP1, Nm
T_{out_MP2}	Output moment CS at MP2, Nm
K_{H_α}	Transverse Load Factor
K_{H_β}	Face Load Factor
Y_{F}	Form Factor
Y_{S}	Stress Correction Factor
$Y_{\delta relT}$	Relative Notch Sensitivity Factor
Y_{NT}	Life Factor for Tooth Root Stress
Z_{R}	Roughness Factor
Z_{NT}	Life Factor for Contact Stress

Acronyms:

Demon-strator	Gearbox including variator machines to be tested
Planetary stage 1	Single planetary stage – Input stage
Planetary stage 2	Single planetary stage – Output stage
CVT	Continuously Variable Transmission
FMPC	Fuzzy Model Predictive Control
FMEA	Failure Mode Effect Analysis
LTCA	Loaded Tooth Contact Analysis
VTOL	Vertical Take-Off and Landing
MP1	Mechanical point 1 - The variator machine D stands still
MP2	Mechanical point 2 - The variator machine C stands still
TSE	Turboshaft engine
IM	Intermediate stage

CS	Compound Split - Consists of the two planetary stages (Planetary stage 1 & Planetary stage 2), the two variator gearboxes (VGBc & VGBd) and electric variator machines (Vc & Vd)
Vc	Variator machine C – Generator
Vd	Variator machine D – Motor
VGBc	Variator gearbox C: Gearbox between planetary stage 1 and variator machine (Vc)
VGBd	Variator gearbox D: Gearbox between planetary stage 2 and variator machine (Vd)
BG	Bevel gearbox
PG	Planetary gearbox

2. INTRODUCTION

The necessity for variable rotor speed technologies is indicated in different research and development projects in the USA, in Europe and in Russia. There are two major research programs, one is the USA ”Future Vertical Lift” (FVL) [1] program and the second is the European Union’s ”Clean Sky 2 - Fast Rotorcraft” program [2]. The aim of both programs is to develop a high-speed rotorcraft with excellent hover and vertical take-off and landing (VTOL) capabilities. In these programs the commonly used single main rotor and tail rotor configuration is not the only configuration of interest. New configurations, like compound rotorcraft or tiltrotor rotorcraft, are under development.

The Airbus Helicopters high speed demonstrator X3, the previous design to the RACER, is a good example for this development. The X3 is a compound rotorcraft with one single main rotor and two tractor propellers mounted on small wings on each side of the rotorcraft. High speed and highly efficient results could be obtained with a speed reduction of the main rotor during forward flight while additional thrust was provided by the two tractor propellers and the wings provided additional lift. The main rotors rotational speed was reduced by the variability of the turboshaft engine in fast forward flight to overcome the problem of high-speed stall on the advancing rotor blade. This setting enabled the X3 demonstrator to achieve an unofficial level-flight speed record of 255kt (472km/h) in June 2013 [3]. The Airbus RACER, optimized for a speed of more than 400 km/h had its maiden flight in April of 2024 [4]. Next to Airbus RACER, the NextGen Civil Tiltrotor by Leonardo is the second demonstrator for Clean Sky 2- Fast Rotorcraft [5]. It is currently in its final assembly and its first flight is projected to be this year [6].

The National Aeronautic and Space Administration (NASA) Heavy Lift Rotorcraft System Investigation [1] is a good example for the possible increase of efficiency with rotor speed variation. Three different passenger transport rotorcraft configurations were investigated. The so called Large Civil Tiltrotor Concept, a tiltrotor rotorcraft, was identified with the highest potential. It needs a rotor speed variation range of about 50% of the nominal RPM to be economically competitive.[7]

Boeings A160 Hummingbird is another good example for improved rotorcraft efficiency due to rotor speed variation. The rotorcraft set up a new record in endurance flight (18.8h) in its class in May 2008. It was possible due to a two stage transmission gearbox for rotor speed variation [8]. Furthermore the rotor and rotor blades were designed by Karem to enable an operation at different RPM [9].

VARTOMS (Variable Rotor Speed and Torque Matching System) is an invention from Airbus Helicopters for the H145 to reduce noise, especially in urban areas, and to improve handling qualities. A speed range of 7% (from 96.5% to 103.5%) of the nominal RPM is possible [10]. A similar system is also used in the Mi-8 class helicopter and its modifications [11].

G.A. Miste presented an optimisation of variable turbo shaft engine performance with main rotor interaction of the T-700 UH-60A engine and the UH-60A main rotor in his doctoral thesis [12]. He concluded that the RPM variation has a significant impact on the specific fuel consumption (SFC) of the turboshaft engine. The main rotor RPM variation performed by the turboshaft RPM variation is less efficient than an independent optimisation of the main rotor RPM and turboshaft engine RPM.

There are three reasons for the trend to rotor speed variation as the previous examples showed. The first reason is the possibility to overcome the divergent requirements on the rotor speed in hover and in fast forward flight. This is especially interesting for the new rotorcraft configurations, like compound rotorcraft or tiltrotor rotorcraft. The second reason is the ability to reduce the emitted noise of the rotorcraft.

This can increase the acceptance of rotorcraft in urban areas and in the surrounding of heliports. The third reason is the efficiency increase of the rotorcraft due to rotor speed variation which reduces the environmental impact.

An investigation of possible benefits of variable rotor speed was performed by H. Amri et. al. [13]. In a CAMRAD II simulation model of a CS-27 class helicopter a required power reduction of 23% could be achieved and different technology categories to enable rotor speed variation as well as the major risks and problems were identified.

W. Garre et. al. [14] analysed the possible efficiency increase and enhancement of the flight envelope with rotor speed variation for five different rotorcraft configuration: a single main rotor, a coaxial rotor, a coaxial compound, a tandem and a tiltrotor configuration. They could show that a rotor speed variation of up to 50% of the nominal RPM is useful for all rotorcraft configurations, but there are always some flight states where rotor speed variation is not suitable. This is at the original design region of the rotorcraft, where the reference rotor speed is equal to the optimum rotor speed.

The technology categories, defined in [13], were explored by H. Amri et. al. [15]. They found out that nowadays only two technologies are suitable for rotor speed variation: the turbine technology and the gearbox technology. An electric drivetrain is an interesting option, but the components are too heavy. The turbine technology adds less additional weight, but it influences the whole drivetrain and the auxiliary units. Gearbox technology is heavier but has the advantage that the RPM of different rotors can be adjusted separately, and the turboshaft engine can be operated at the optimum speed as well. RPM variation with the turbine technology is suitable for a small variation range while gearbox technology is suitable for a large variation range.

W. Garre et. al. [16] analysed the rotor speed variation in the context of missions for five different rotorcraft configurations. They made a comparison between a single rotor speed, a two speed and a continuously variable transmission (CVT) variant within the missions. CVT systems showed the best benefits for utility rotorcraft. For fast rotorcraft, like compound or tiltrotor rotorcraft, the two speed transmission gains almost the same benefits as the CVT. For all configurations an efficiency increase could be identified.

P. Paschinger et. al. [17] explored three different gearbox technology groups: discrete variable gearboxes, pure CVT gearboxes and power split gearboxes. They concluded that power split gearboxes are most suitable for rotor speed variation and within this group the compound split gearboxes are the favourable solution. A functional Failure Mode Effect Analysis (FMEA) of the compound split indicated no additional risks in the drivetrain for a rotorcraft which could not be negated with additional measures.

An investigation of the kinematic behaviour and the mass of different compound split configurations was performed by H. Amri et. al. [18]. The investigation showed that the power flow in the variator path is the same for all configurations and it depends only on the spread (ratio of highest output speed to lowest output speed). The mass of the compound split configurations is different and depends on the basic transmission ratio (ratio of the input speed to the highest output speed) and the spread. They concluded that a compound split variation is most suitable when it has the lowest mass at a high basic transmission ratio in a given range of spread.

P. Paschinger et. al. [19] investigated the reliability of two different drivetrain architectures, each containing a compound split. Furthermore, they did examinations on different possible variator engines for the compound split.

Bischläger et al. [20] focused on the simulation model of the turbine engine and selecting optimal variator machines, concluding that electric variators provide the best efficiency, mass, and reliability balance.

Scheu et al. [21] [22] investigated the dynamic simulation of the complete drivetrain including a fuzzy model predictive control (FMPC) approach for rotor speed control and vibration damping.

Since the research results to date show the suitability of the Vari-Speed gearbox concept for use in helicopters, this paper develops the plan for the functional verification of the gearbox concept.

The questions that are answered in the present paper are:

1. How can a gearbox be scaled to a smaller size, for easier testing, while retaining a similar behaviour as the full-size transmission.
2. How can the function of the compound split variable speed gearbox be demonstrated on a test stand.

3. Methodology

3.1. Compound Split Transmission

A compound split gearbox for rotorcraft speed variation is described in Amri et al. [18] and consists of two planetary gear sets as displayed in Figure 1. The planetary gears have one common shaft (1) and four shafts that need to be constrained. The input (1) and output shafts (3) of the compound split provide two constraints. The remaining two rotational degrees of freedom are defined via a helical gear stage between the ring gears and the variator generator (4) as well as the variator motor (5). The carrier shaft of the first planetary gear is connected to the ring gear of the second planetary gear (2). The variator generator and variator motor can be imagined as a trans-mission that provides a ratio of 0 to – infinity between the two shafts (4) and (5) of the compound split.

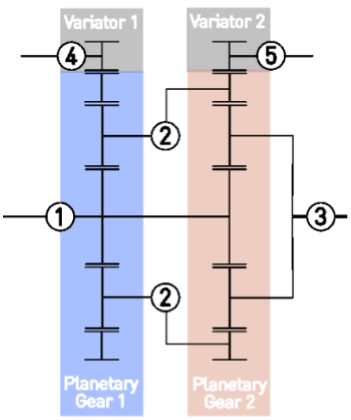

Figure 1: Compound Split schematic

In the presented model, two electric machines are used as variator motor and generator. By varying the RPM of the electric machines RPM variation of the output shaft of the compound split is achieved. In this power split configuration, the power is transferred through the highly efficient mechanical path (gear contact) and the electric path (electric machines). The power that is transferred through the electrical machines (Equation (1)) is dependent on the desired range of RPM variation: the spread **R** [17].

$$P_{var,\,max} = \frac{\sqrt{R}-1}{\sqrt{R}+1} * P_{TSE} \tag{1}$$

Figure 2 (upper) shows the results of for a spread of 1<R<3: A transmission ratio spread of R=1.5 would lead to approximately 10% of the total input power being transmitted through the electrical path. Figure 2 (lower) depicts, how much relative power is being transmitted through the electrical path for each transmission ratio. The mechanical points MP1 & MP2 describe defined transmission ratios of the compound split where one electric machine stands still, while the other turns without transmitting torque. For these MPs, no electric power is transferred through the electric path: The power transfer takes place solely through the mechanical part of the compound split and is highly efficient.

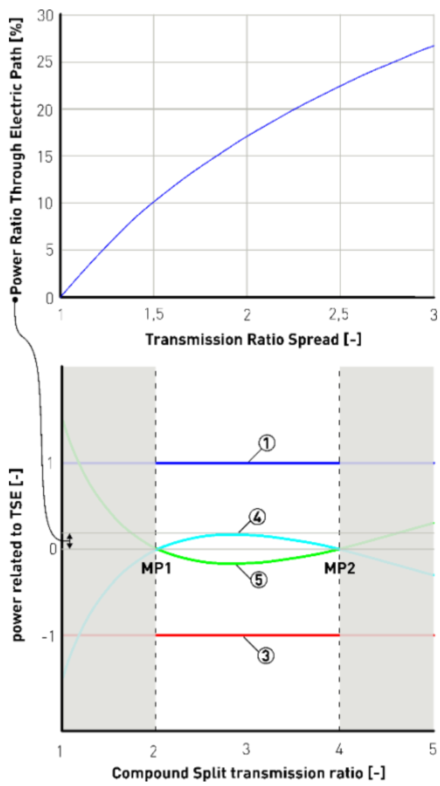

Figure 2: (upper) power ratio through electric path dependent on the spread, (lower) normalized power flow through each shaft of the compound split dependent for a spread of R=2.

There are several options to include a compound split within the drivetrain of a helicopter, which are described in Amri et al. [18] In this publication, the compound split is located between the input stage (IM) and the bevel gear stage (BG). This means that for each turboshaft engine (TSE) one compound split is necessary.

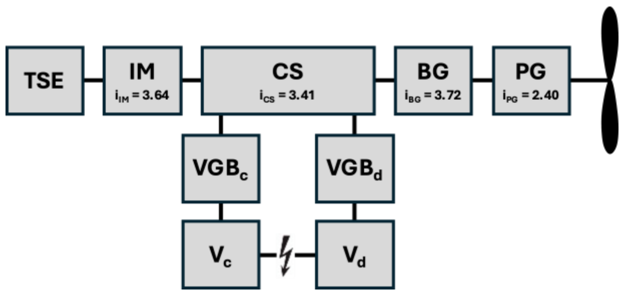

Figure 3: Architecture of the helicopter powertrain for one TSE

The chosen configuration of PG transmission ratios, leads to a low mechanical point at 2.27 (MP1) and a high mechanical point at 3.41 (MP2).

3.2. Scaling method

The validation tests are planned to be conducted on the E-Mobility test stand developed and built by *Zoerkler Gears GmbH.* This test stand was originally designed for testing electric axles for road vehicles but its flexible layout allows testing of complete drivetrains, gearboxes, and individual gear stages. The test stand features one 265 kW electric machine and two 340 kW machines, providing ample power for simulating various operating conditions. A 400 kW 1200 V DC battery simulator is available to supply power to electrical machines. The test stand is controlled by the KSengineers Tornado automation system, which enables control of the test stand machines and data acquisition from various sensors.

The power of one of the T700 turbines of the UH60 helicopter, used as the basis for the investigations, has a continuous power output of 1239 kW and a peak power of 1447 kW [23]. This far exceeds the capabilities of the test stand. Also, considering the safety during test execution and the costs of a demonstrator, testing in this power class is unfeasible for the current development stage of Vari-Speed.

For this reason, a scaling methodology was developed to make statements about the function of the full-scale system through tests of a scaled-down demonstrator gearbox. The requirements for the scaling method are:

- Equal gear safety factors (< 5% deviation)
- Equivalent dynamic behaviour (Eigenfrequencies scale with scaling factor, shapes of the eigenmodes are similar)

To avoid costly and time-consuming simulations or prototype realizations, Similarity Theory methods are used today. These allow quick and efficient determination of a system's behaviour and functionality when its size is altered. The main methods of Similarity Theory are dimensional analysis and scaling approaches. These provide highly effective tools for making generally valid statements about how relevant physical quantities in systems change when geometric dimensions are modified or materials are substituted. [24]

Nam et al. [25] suggested the usage of Similarity Theory to scale a 2MW wind turbine gearbox to quarter its size. Their model was validated by comparing the load capacity parameters which showed only a small difference of 2% in tooth root and contact stresses.

Zhang et al. [26] further researched the prediction of the dynamic behaviour of transmissions based on scaled models. They concluded that the vibration displacement, acceleration and meshing forces of the full sized model can be predicted with good accuracy.

Weinberger et al. [27] worked on a scaling method for a planetary gear stage with the purpose of keeping the excitation of the meshing gears similar to the original gearbox. This leads to a similar noise behaviour.

Based on the results of these investigations, it was decided to scale the demonstrator gearbox using the Similarity Theory. If L is set as the ratio of the lengths of the original size to the size of the test specimen, the result is that the forces scale with a ratio of L^2 and the torques with a ratio of L^3 [24]. The advantage of scaling according to this method is that many basic characteristics of the gearbox, such as number of teeth, tooth shape, etc., can remain constant and only the dimensions, such as tooth modulus and tooth width, need to be changed. Since the eigenfrequencies are inverse proportional to size, and a goal is to keep the ratio of resonance speed to operating speed similar, the rotational speeds need to scale with 1/L. In order to achieve a stress similarity the gears should be manufactured with the same material, heat treatment, and quality grade, as well as the same geometric shape [25].

The scaling method was tested in the gear calculation software KISSsoft® using a model of a single-stage gearbox. A model scaled to half the size of this gearbox was compared with the full-size model. In this model Gear 1 is the smaller pinion and Gear 2 is the big gear.

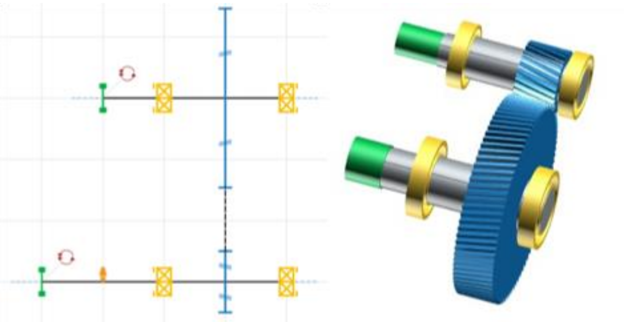

Figure 4: Test model for scaling method

With this model a gear load capacity calculation according to *ISO 6336* [28], [29], [30], as well as a shaft calculation according *DIN 743* [31] was performed. Further analyses were also carried out, including a contact analysis of the gearbox and a modal analysis of the system.

For the calculation of the gear load capacities, the face load factor K_{H_β} and the transverse load factor K_{H_α} were fixed. This was done, since the calculation of these factors is also dependent on the stiffness of the housing and other components of the gearbox, that were neglected in the development of the scaling method. Also these factors can be influenced by adapting the micro geometry of the gears which is not considered at this stage.

Differences in safety factors for tooth bending stress can be explained by a higher tooth root stress due to higher Form Factor Y_F and stress correction factor Y_S as well as a slightly lower permissible strength due to slight differences in the relative notch sensitivity factor $Y_{\delta relT}$ and life factor for tooth root stress Y_{NT}.

Table 1: Results of the tooth root safety calculation

		Half-size	Full-scale
Gear 1	Tooth root stress [N/mm^2]	441.95	434.43
	Permissible tooth root stress [N/mm^2]	740.34	751.02
	Safety factor for tooth root stress	1.68	1.73
Gear 2	Tooth root stress [N/mm^2]	498.47	481.46
	Permissible tooth root stress [N/mm^2]	757.93	769.09
	Safety factor for tooth root stress	1.52	1.60

The results of the surface durability (pitting) calculation seen in Table 2 of the test model shows no difference between the half-scale model and the full-size model in the actual contact stress. The differences in permissible contact stress are due to deviations of the roughness factor Z_R and the life factor for contact stress Z_{NT}.

Table 2: Results of the surface durability calculation

		Half-size	Full-scale
Gear 1	Contact stress [N/mm^2]	1370.84	1370.63
	Permissible contact stress [N/mm^2]	1331.03	1384.99
	Safety factor for contact stress	0.97	1.01
Gear 2	Contact stress [N/mm^2]	1370.84	1370.63
	Permissible Contact stress [N/mm^2]	1381.94	1437.97
	Safety factor for contact stress	1.01	1.05

The shaft calculation showed a similar bending shape. The maximum deflection of the half-size model is 45% of the deflection of the real size model which corresponds to a deviation of 10%. The curve and amplitude of the equivalent stress are identical for the original size model and the scaled model as shown in Figure 5.

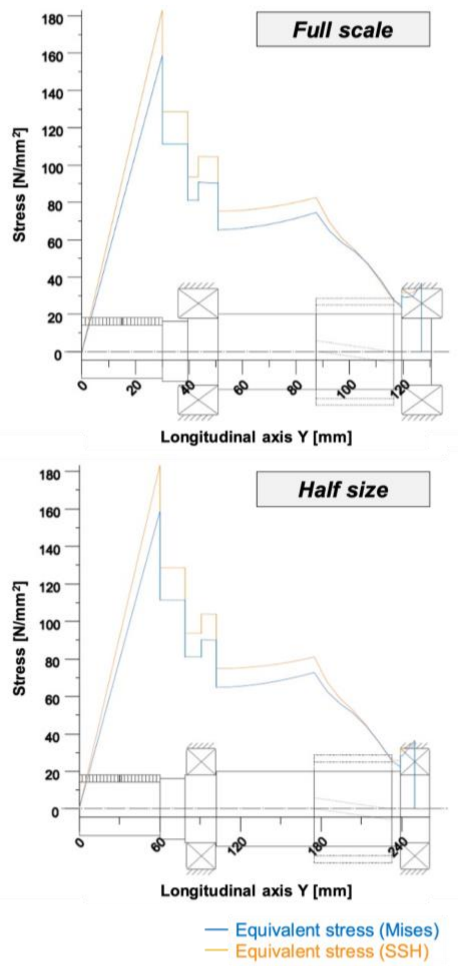

Figure 5: Comparison of equivalent stresses. (upper) Full-scale model, (lower) Half-size model

Loaded Tooth Contact Analysis (LTCA) is crucial for understanding the deformation of gears and its effect on various factors such as noise excitation, contact pattern, contact shocks and torque variations. The contact analyses of the full-scale and the half-size model show a very good match. The peak-to-peak transmission error, which is often used as an indicator for the NVH-behaviour of a geared transmission scales with the scaling factor, as can be seen in Figure 6. The tooth root stress under load calculated with LTCA and the contact stress are similar between full-scale and half-size model.

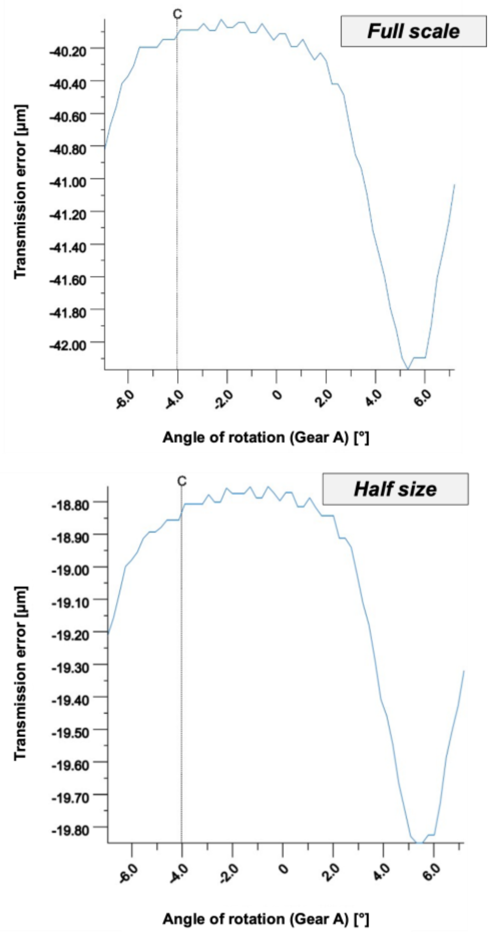

Figure 6: Comparison of peak-to-peak transmission error. (upper) Full-scale model, (lower) Half-size model

Bearing life is not directly comparable, as simple scaling of bearings based on the Similarity Theory is not feasible. Especially in aerospace applications, standard rolling bearings are rarely used, rendering calculations according to *ISO/TS 16281* [32] of little significance. The complex operating conditions in aircraft, including temperature fluctuations, high rotational speeds, and variable loads, as well as the focus on low weight require specially developed bearings with adapted materials and geometries. Additionally, factors such as lubrication, contamination, and dynamic loads play a crucial role, which cannot be easily scaled.

A comparison of the eigenfrequencies of the shafts from the test model show that the calculated frequencies of the half-scale model and the frequencies predicted by multiplying the eigenfrequencies of the full-scale model by the scaling factor are matching. If bearing stiffnesses are taken into account, the eigenfrequencies can deviate, due to the difficulty of scaling the bearings.

Furthermore, the results for the eigenfrequencies were compared between KISSsoft® and an analysis in Simcenter 3D™. The first ten natural eigenfrequencies were compared. This showed that the deformation curves at the same frequencies are identical between the two programs. The results of the displacements for the eigenfrequency of *2760 Hz* and *2646 Hz* from KISSsoft® and Simcenter 3D™ are shown in the Figure 7. In KISSsoft®, the displacements for the respective eigenfrequency are normalised to the radius of the shaft.

Comparing the scales of the two graphs, it can be seen that the normalised displacement is calculated in KISSsoft®. The displacement is normalised using the maximum displacement of the total calculated natural frequencies. By comparing the two figures from KISSsoft® and Simcenter 3D™ it can be seen that the forms of the bending lines are the identical.

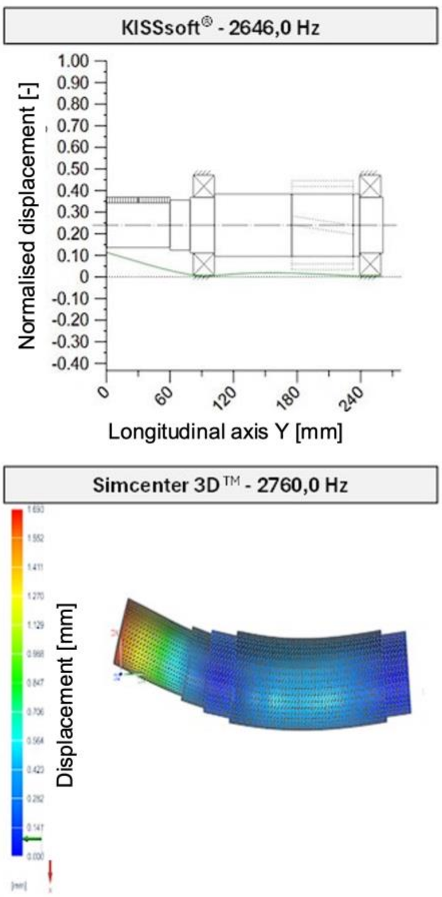

Figure 7: Comparison of the deformation curves at *2646 Hz* and *2760 Hz*

The root mean square deviation of the frequencies between KISSoft and Simcenter 3D is 7,2%, while the maximum deviation between the frequencies is 14%. Results of the natural frequency analysis are summarised in Table 3. The deviation can be explained by the deviation in the modelling of the bearings between KISSsoft® and Simcenter 3D™. In Simcenter 3D™, the entire surface of the bearing seat is fixed. In KISSsoft®, only the centre point of the bearing is fixed.

Table 3: Eigenfrequencies of the test model

Eigenfrequencies - Input shaft spur gear

	Simcenter 3D	KISSsoft	Deviation KISSsoft - Simcenter 3D
No.	Frequenz in Hz	Frequenz in Hz	Percentage
f1	0,0023	0	2,3
f2	2760	2646,0	4,1
f3	5061	4712,1	6,9
f4	7916	7032,1	11,2
f5	12390	12528,4	-1,1
f6	12680	12791,0	-0,9
f7	15590	14091,9	9,6
f8	15060	15214,1	-1,0
f9	19030	20137,5	-5,8
f10	23490	20230,9	13,9

4. RESULTS

4.1. Scaling method

The scaling factors chosen to keep the performance of the demonstrator below the maximum values allowed by the test bench are as follows:

Table 4: Chosen scaling factors

Characteristic	equation	Scaling factor
Length	L	0.385
Force	L^2	0.148
Torque	L^3	0.057
Rotational speed	1/L	2.597
Power	L^2	0.148

With these chosen scaling factors, the input and output data of the demonstrator gearbox are shown in Table 5.

Table 5: Input and output data of original and scaled demonstrator

	Original size	Scaled Demonstrator
n_{in} [rpm]	5750	14935
T_{in} [Nm]	1625	92.7
P_{in} [kW]	978.5	145
T_{out_MP1} [Nm]	5532	315.7
T_{out_MP2} [Nm]	3688	210.5
n_{out_MP1} [rpm]	1689	4387
n_{out_MP2} [rpm]	2533	6579.2

Figure 8 shows the amount of power that is transmitted via the variator path if no losses are assumed. In the mechanical points at a transmission ratio of 2.27 and 3.41 the complete power is transmitted via the mechanical path, while at a transmission ratio of about 2.8 about 14.6kW (10% of input power) is transmitted via the variator path.

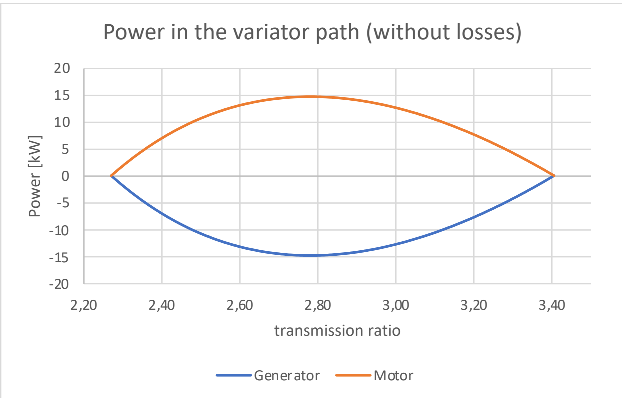

Figure 8: Power in the variator path over whole speed range

The scaled demonstrator was designed in the gear calculation software KISSsoft®[33]. The compound split designed by Scheu et al. [21] was used as a basis for the scaled gear geometry. The gears were designed with gear modules from the standard series to be manufactured by standard tools. This was done to keep manufacturing costs down. The demonstrator is not optimized for low weight, as the weight only plays a minor role for the functional and safety verifications on the test bench. Figure 9 shows the design of the KISSsoft® model, the associated input parameters and calculated safety factors are summarised in Table 6.

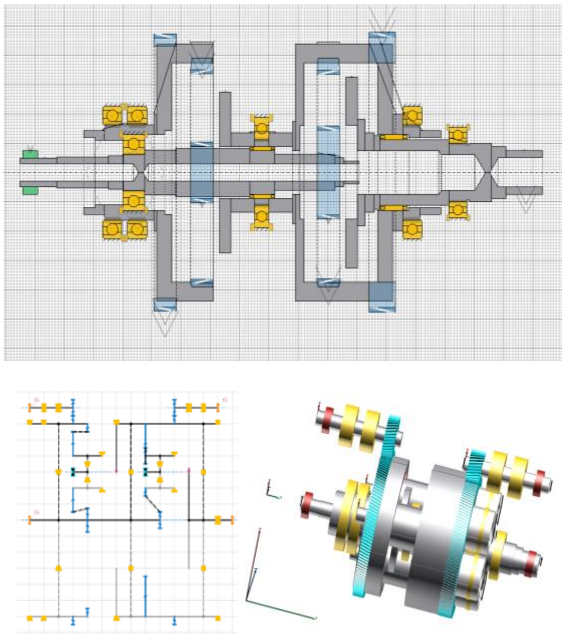

Figure 9: Design of the demonstrator in KISSsoft®

Table 6: Safety factors and input parameters of the KISSsoft® model

Main component	Element	SF	SH
Variator C	Gear	**2.530**	**1.551**
	Pinion Gear	**2.655**	**1.492**
Variator D	Gear	**2.886**	**1.346**
	Pinion	**3.063**	**1.286**
Planetary gearbox C	Sun Gear	**13.809**	**2.472**
	Planet Gear	**9.728**	**2.510**
	Ring Gear	**14.263**	**4.781**
Planetary gearbox D	Sun Gear	**6.562**	**1.830**
	Planet Gear	**4.267**	**1.839**
	Ring Gear	**5.930**	**2.628**

Coupling	Moment (Nm)	RPM	Power (kW)
Turboshaft engine	92.7	14935.0	145.0
Rotor	-268.4	5154.0	-144.9
Variator C	-15.0	8986.8	-14.1
Variator D	-27.4	-4866.0	14.0

4.2. Demonstrator-Gearbox

The aim of the demonstrator is a cost-effective design that is suitable for proving the function of the Vari-Speed concept on the test bench.

Figure 10 shows the architecture of the demonstrator-gearbox. The main components are the compound split, which consists of two mechanically linked planetary gearboxes, variator shaft C and variator shaft D. The two variator strands each consist of the gear stage, the variator shaft, the brake system and the electric variator machine.

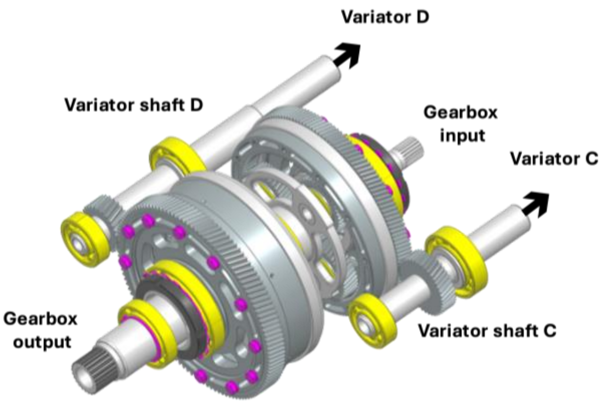

Figure 10: Architecture of the demonstrator-gearbox

The dimensioning of the bearings and the calculations of the losses and lifetimes of the roller bearings were performed with the KISSsoft® calculation tool. The bearings were designed for the demonstrator. As already mentioned in chapter 3.2, it is not possible to scale the bearings using the specified methods. The design of the bearings in their original size does not represent the scope of the project. In the bearing concept, a distinction is made between the three main components compound split, variator shaft C and variator shaft D. The two variator shafts are supported by two angular contact ball bearings in an O-arrangement in the gearbox housing. The greater challenge, of course, is the bearing support for the compound split. The compound split is supported via five bearing locations in the gearbox housing. The sun shaft is supported entirely by the internal bearings in the ring gear of the input stage and in the connection section between the planet carrier of the input stage and the ring gear of the output stage. This bearing concept is shown in Figure 11.

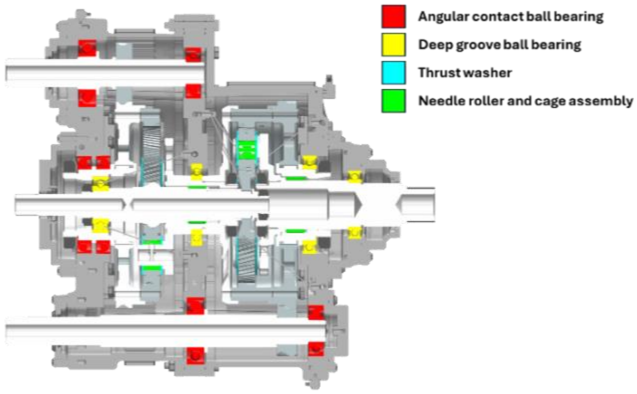

Figure 11: Bearing concept of the demonstrator

The bearing seats on the shafts and in housing parts were designed according to the specifications of the bearing manufacturer SKF. The gearing was designed according to the scaled dimensions using KISSsoft® [33].The calculation model from KISSsoft® required for this is shown in Figure 12. The tooth root and flank strength are calculated using the calculation method of *ISO 6336:2019* [28], [29], [30]. The scaled shafts are calculated using the *DIN 743:2012* [31] calculation method.

When selecting and designing the rotary shaft seals, particular attention was paid to compliance with the maximum permissible speed of the components. This presented a challenge, as the speeds of the input shaft and the two variator shafts have a maximum speed of up to 15.000 RPM. This challenge was overcome by adapting the shaft diameters and using high speed radial shaft seals.

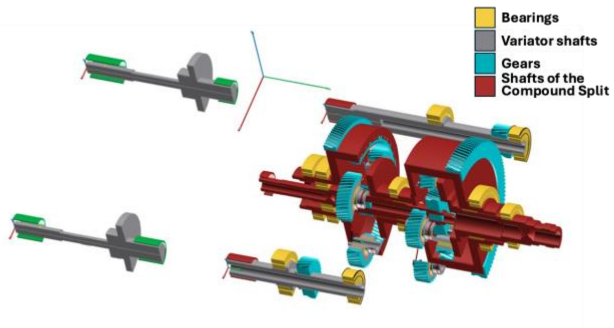

Figure 12: Calculation model from the calculation tool KISSsoft®

Commercial permanent magnet synchronous machines were selected as the electric variator machines. To minimize the load on the electric variator machines which are standing still at the mechanical points, brake discs are mounted on the variator shafts.

The gearbox housing consists of 10 main parts, including 4 housing sections and 6 housing covers.

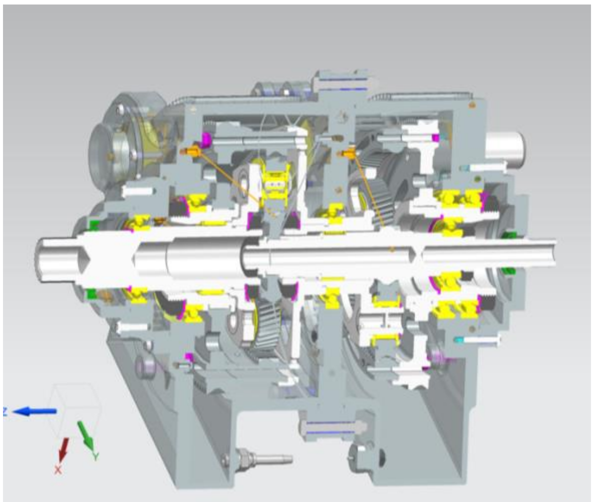

Figure 13: Cut-View of Demonstrator Gearbox

The Vari-Speed II demonstrator gearbox's losses and required cooling capacity are derived from analysis of its full-scale counterpart. The full-scale gearbox concept uses a Helix CTSM242-01(HV) [34] electric machine, whose efficiency map closely matches earlier calculations.

Figure 14 shows the power in the variator path for the full-size drivetrain. The electrical losses at full power are constant at about 20kW over a wide range of rotor speed. This is due to the lower efficiency of the electric machines near the mechanical points.

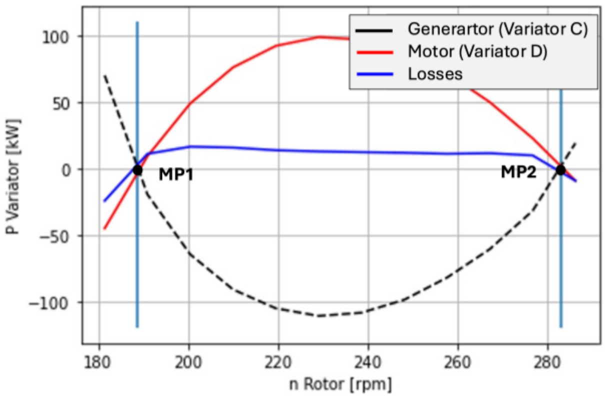

Figure 14: Power in the variator path including losses

The mechanical path is assumed to have a 97% efficiency. In mechanical points, where all power flows through the mechanical path, no variator losses occur.

Calculations show:

- Input power: 980kW
- Output power at mechanical points: 950.6kW
- Mechanical losses: 29.4kW
- Total losses: 49.4kW (29.4kW mechanical + 20kW variator)
- General output power: 930.6kW
- Overall efficiency: 95%

For the demonstrator, losses are scaled down by a factor of $L^2 = 0.148$, resulting in:

- Scaled variator losses: 2.96kW
- Scaled mechanical losses: 4.35kW
- Maximum scaled losses: 7.31kW

The planned test stand's cooling unit has a maximum capacity of 9 kW, sufficient for the demonstrator's needs. To dissipate the electrical losses in the variator path, a coolant mass flow of at least 0.09 kg/s is required, assuming a 10 K temperature difference between inlet and outlet.

4.3. Test Planning

The propulsion system developed in the Vari-Speed project represents a new system that has not yet been implemented in practical aviation applications. In the aerospace industry, safety is paramount, and validation is essential before any new system can be deployed. The safety requirement necessitates a test campaign for the further development of the system.

This chapter focuses on the initial phase of the testing process: the creation of a detailed test plan for the demonstrator.

The goal of the test plan is to define experimental investigations that demonstrate the functionality of the system and the behaviour under off design conditions.

The first step was to analyse the regulatory requirements for the construction and testing of helicopter gearboxes. The main focus here was on the *EASA CS29* [35] and its *FAA counterpart*, the *AC29* [36]. Rotor speed variation is a topic that is not yet widely regulated by the governing authorities, but there are first specifications for testing of helicopter with more than one gear.

CS29.923 (n) in particular should be emphasised here: “Special tests. Each rotor drive system designed to operate at two or more gear ratios must be subjected to special testing for durations necessary to substantiate the safety of the rotor drive system."[35]

Section 29.923(n) of the FAA AC29 is more precise with the requirements. It requires: "special tests for rotor drive systems designed to operate at two or more gear ratios. Depending on the limitations and instructions proposed for operating at other gear ratios, additional tests (beyond the normal 200-hour schedule) or substitutions into the basic test should be conducted to qualify the rotor drive system for operations at other gear ratios. The duration of testing, torque and speed requirements, overspeed tests, and control positions for these tests should parallel the requirements of the basic endurance test."[36]

EASA AMC1 29.927 describes additional required tests for drivetrains with variable rotor speed: "In order to substantiate an acceptable vibration and dynamic behaviour of rotor drive systems when using the available range of rotor speeds within the variable NR (rotor speed) function, the applicant should consider performing specific test investigations, as prescribed in CS 29.927(a). The need for representative test runs at the different torque and rotor speed combinations, covering steady states and transient conditions to be encountered in operation, should be evaluated by and agreed with the Agency." [35]

With this in mind, various tests were defined to prove the functions of the gearbox concept under different conditions. The demonstrator gearbox will be equipped with several temperature and acceleration sensors to record the temperature of the components and vibrations during operation, as well as the oil temperature on different positions (see Figure 15). Furthermore, combined torque and speed sensors (HBM T40B [37]) will be provided at the input and output of the demonstrator gearbox. Torque-speed sensors (HBM T210 [38]) will also be installed in the variator path to measure the losses in the variator path.

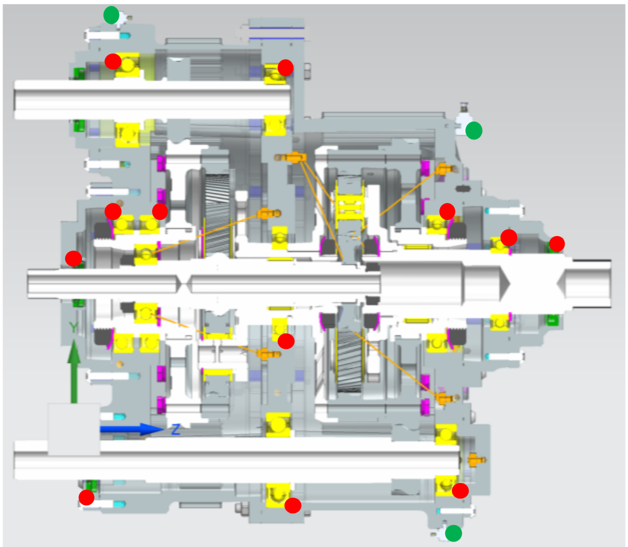

Figure 15: Position of vibration sensors (green) and temperature sensors (red) on demonstrator

Figure *16* shows the interfaces of the demonstrator on the test bench. The mechanical part of the demonstrator is highlighted in grey. VA_D and VA_C are the variator machines with their respective Inverters INV_C and INV_D. M1 and M2 are the electric machines of the test bench with their reducing gearboxes highlighted in red.

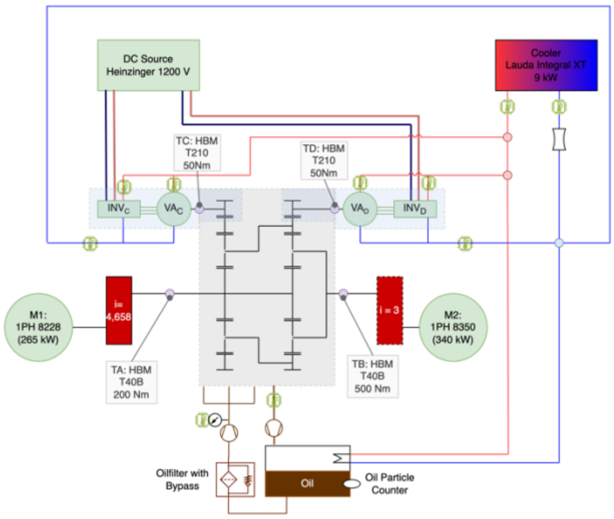

Figure 16: Interface diagram of the demonstrator

Figure *17* shows the entire test setup for the demonstrator on the test bench, which is connected to the input and output machines.

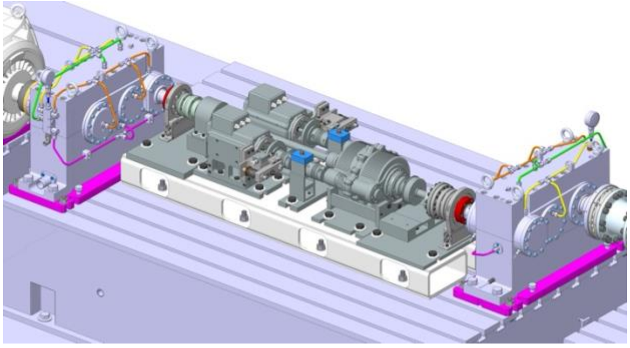

Figure 17: Demonstrator on the testbed

Testing of the Vari-Speed II Demonstrator consists of the following test sequences:

Commissioning of the gearbox to verify its fundamental functions and assess its performance at the mechanical points. This initial evaluation ensures that all components are functioning as designed and provides a baseline for subsequent tests.

Test of the rotor speed variation to examine the gearbox's ability to operate across a range of speeds and to transition between them efficiently. This testing sequence is conducted as follows:

a) Fixed Speed Operation: The gearbox is initially operated at various fixed speeds to establish baseline performance metrics.

b) Gradual Speed Changes: Slow changes in rotational speed are introduced to evaluate the functionality of the speed control system and the variators.

c) Accelerated Speed Changes: Tests are conducted with increasing rates of speed change at different output power levels to determine the maximum rate of change achievable.

d) High-Power Testing: At high drive powers, the power surplus of the variator machines may not be sufficient to overcome the system's inertia for rapid speed changes. To identify these limitations, the temperatures, temperature changes in the variator machines, and torque at the variator shafts is monitored. The maximum rate of change is considered reached when the windings of the variator machines attain their maximum allowable temperature.

Test of the hybrid mode: The incorporation of electric variator machines enables the expansion of the system into a hybrid configuration. This mode allows power to be extracted from the compound split gearbox via the generator and stored in a battery, which can later be fed back through the motor. To demonstrate this functionality, the following test is conducted: The gearbox is operated at a constant input speed, with the variator machines regulated to maintain a set output speed. When a higher power is introduced into the gearbox by the test stand's drive machine, the excess must be fed into the battery via the generator. This test verifies the system's ability to manage power flow effectively in hybrid mode**.**

Tests of the Vibration damping

Part of the Vari-Speed project is a flight test campaign that is conducted using the helicopter technology simulator at the *Technical University of Munich*. This campaign allows for the recording of rotor loads occurring during various flight maneuvers. These recorded loads provide an opportunity to simulate real flight conditions on the gearbox test stand, enabling an investigation of the demonstrator gearbox's behaviour under authentic loading scenarios.

The loads recorded on the flight simulator correspond to a full-scale helicopter and must be scaled to the demonstrator using the developed scaling methodology. The objective of this test is to replicate several complete flights on the test stand. The impedance control implemented on the test stand allows the drive and output electric machines to behave as they would in a real helicopter system, mimicking the characteristics of the turbine and main rotor gearbox connected to the rotor.

Testing under off-design conditions and component failure tests

As part of the test planning, the failure possibilities and probabilities of the transmission were also investigated. Special attention was given to the electrical components, as these constitute the biggest difference compared to a normal helicopter transmission. These investigations also serve to explore possibilities for minimizing these risks through additional components, special control systems, and design adjustments.

The basis for the investigation of failure probabilities is the work "*Hazards Analysis and Failure Modes and Effects Criticality Analysis (FMECA) of Four Concept Vehicle Propulsion Systems*"[39]. In this study, four novel aircraft configurations with electric or hybrid propulsion systems were examined for their failure probability.

For the investigation of the Vari-Speed system, a Functional Block Diagram was created, in which all functions of the drive are indicated as blocks. This diagram serves as the basis for an FMECA. The components Turbine (TSE), Rotor, and the Flight Control System are not part of the failure probability investigation, as these have been in use in helicopters for many years and have already proven their reliability. The functions shown in Figure 18 are as follows:

- Function 1: Transfer TSE torque to Rotor
- Function 2: Convert torque at shaft C to electrical energy
- Function 3: Provide battery storage of electrical energy
- Function 4: Convert electrical energy to torque at shaft D

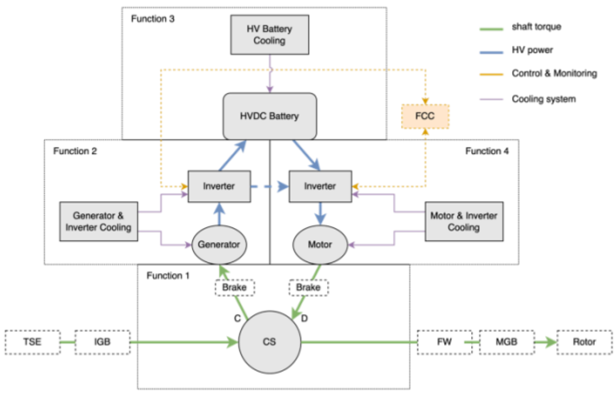

Figure 18: Functional block diagram of Vari-Speed Transmission

Based on the Functional Block Diagram, the failure rates of the individual components were investigated, and a Failure Mode and Effects Criticality Analysis was created. The failure modes are divided into individual categories according to severity. These classes are shown in Table 7.

Table 7: Explanation of failure mode categories

Cat.	Severity of effect
I	Catastrophic: A failure which can cause death or system loss.
II	Critical: A failure which can cause severe injury, major property damage, or major system damage which will result in mission loss.
III	Marginal: A failure which may cause minor injury, minor property damage, or minor system damage which will result in delay or loss of availability or mission degradation.
IV	Minor: A failure not serious enough to cause injury, property damage, or system damage, but which will result in unscheduled maintenance or repair.

At this development stage only categories I and II were investigated, because these represent the most critical failure modes with the greatest impact on system safety and functionality. The calculated failure rates per flight hour for the individual classes are shown in Table 8:

Table 8: Results of FMECA

Category	Failure rate per flight hour
I	5,05E-06
II	5,00E-09

These results are promising, but they demonstrate that further efforts are necessary to improve the safety of the propulsion system in order to achieve the low risks required in aviation. In particular, the reliability of individual propulsion system components needs to be increased. These components presumably must have a failure rate of less than 10^{-10} per flight hour in order to meet the requirement of CS29.1309 [35] that a catastrophic failure is extremely improbable (less than 10^{-9} per flight hour).

The off-design condition and component failure tests focus on the behaviour of the transmission under autorotation, OEI-operation with higher load on the compound split and the behaviour if a partial or complete failure of an electric machine in the variator path occurs. Also, the degradation of performance under failure of the cooling system will be investigated.

5. CONCLUSIONS

1. The deviation of the calculated gear safety between a model scaled using the developed scaling method and a full-size model is less than 5%. This indicates that gear results obtained from scaled models can be extrapolated for further analysis and development.

2. The eigenfrequencies predicted by the scaling method closely match calculated values and modes.
3. With the designed scaled demonstrator and the test sequences defined in the test plan, the function of the demonstrator can be tested in a follow-up project.
4. The results of the preliminary FMECA are promising, but the reliability of the Vari-Speed drivetrain components need to be increased to make failures extremely improbable.

Author contact:

Christopher Gross Christopher.gross@adt-engineering.at

Andreas Juen andreas.juen@adt-engineering.at

Lorenz Braumann Lorenz.braumann@adt-engineering.at

Hanns Amri hanns.amri@adt-engineering.at

6. ACKNOWLEDGMENTS

VARI-SPEED II is a transnational research project, funded in Austria by TakeOff (Federal Ministry of Climate Action, Environment, Energy, Mobility, Innovation and Technology) and in Germany by LuFo, the Federal Aviation Research Programme (Federal Ministry for Economic Affairs and Climate Action).

7. REFERENCES

[1] W. Johnson, G. K. Yamauchi, and M. E. Watts, 'NASA Heavy Lift Rotorcraft Systems Investigation', in *The 2nd International Basic Research Conference on Rotorcraft Technology*, Nanjing, China: NASA, Nov. 2005.
[2] 'Fast Rotorcraft IADP | Clean Aviation'. Accessed: Aug. 19, 2024. [Online]. Available: https://www.clean-aviation.eu/clean-sky-2/programme-overview-and-structure/clean-sky-2-structure/fast-rotorcraft-iadp
[3] M. Hischberg, 'Clean Sky 2 update, part 1: The Airbus Racer', *vertiflite (A Publication of AHS International)*, no. 63, pp. 26–28, 2017.
[4] KS, 'Airbus Helicopters: Highspeed-Helikopter Racer startet zum Erstflug'. Accessed: Jul. 15, 2024. [Online]. Available: https://www.flugrevue.de/zivil/airbus-helicopters-racer-startet-zum-erstflug/
[5] 'Fast Rotorcraft demonstrators due to take to the skies by'. Accessed: Aug. 07, 2024. [Online]. Available: https://www.clean-aviation.eu/fast-rotorcraft-demonstrators-due-to-take-to-the-skies-by-mid-2023-annual-review-meeting-finds
[6] 'Next-Generation Civil TILTROTOR | Clean Aviation'. Accessed: Aug. 07, 2024. [Online]. Available: https://www.clean-aviation.eu/next-generation-civil-tiltrotor
[7] C. W. J. Acree, H. Yeo, and J. D. Sinsay, 'Performance Optimization of the NASA Large Civil Tiltrotor', NASA Ames Research Center, Moffett Field, California 94035, USA, 2008.
[8] G. Plutrich, 'FARNBOROUGH: Cutaway & technical description: Defying convention - Boeing A160 Hummingbird', *Flightglobal*, no. 178(5248), pp. 90–94, Jul. 2010.
[9] A. E. Karem, 'OPTIMUM SPEED ROTOR', US 6,007,298, Dec. 1999
[10] U. D. O. Defence, 'Eurocopter EC145 UH-72 Lakota Helicopter Flight Manual',. 2008.
[11] M. D. Bureau, 'Mi-8-helicopter flight manual'. MIL Design Bureau, 2008.
[12] G. A. Misté, 'Variable Speed Rotor Helicopters: Optimization of Main Rotor Turboshaft Engine Integration', PhD Thesis, Scuola di Dottorato di Ricerca in Ingegneria Industriale, 2015.
[13] H. Amri, R. Feil, M. Hajek, and M. Weigand, 'Possibilities and difficulties for rotorcraft using variable transmission drive trains', *CEAS Aeronautical Journal*, vol. 7, no. 2, pp. 333–344, Jun. 2016.
[14] W. Garre, T. Pflumm, and M. Hajek, 'Enhanced Efficiency and Flight Envelope by Variable Main Rotor Speed for different Helicopter configurations', in *42nd European Rotorcraft Forum 2016*, Lille, France, Sep. 2016.
[15] H. Amri, P. Paschinger, M. Weigand, and A. Bauernfeind, 'Possible Technologies for a variable Rotor Speed Rotorcraft Drivetrain', in *42nd European Rotorcraft Forum 2016*, 2016.
[16] W. Garre, H. Amri, T. Pflumm, P. Paschinger, M. Hajek, and M. Weigand, 'Helicopter Configurations and Drive Train Concepts for optimal Variable Rotor Speed Utilization', in *Deutscher Luft- und Raumfahrtkongress 2016*, Braunschweig, Germany, Sep. 2016.
[17] P. Paschinger, H. Amri, K. Hartenthaler, and M. Weigand, 'Compund-split Drivetrains for Rotorcraft', in *43rd European Rotorcraft Rorum 2017*, 2017.
[18] H. Amri, K. Hartenthaler, and M. Weigand, 'Mass and Kinematic Analysis of Compound Split with Simulation of the Shifting Process for Variable Rotor Speed', in *AHS International 74th Anual Forum & Technology Display*, 2018.
[19] P. Paschinger and M. Weigand, 'Study on possible solutions of a Compound-Split transmission system for the UH-60 helicopter', *Mechanism and Machine Theory*, vol. 129, pp. 17–35, Nov. 2018.
[20] M. Bischläger, C. Gross, and J. Koch, 'Dynamic Simulation of a Rotor System with Variable

Speed’.
[21] T. Scheu, A. Poks, F. Donner, and M. Weigand, ‘Dynamic Simulation of a Rotorcraft Main Transmission with Continuous Variable Ratio’, in *Proceedings of the Vertical Flight Society 79th Annual Forum*, West Palm Beach, Florida USA: The Vertical Flight Society, May 2023, pp. 1–9. doi: 10.4050/F-0079-2023-18148.
[22] T. Scheu, A. Poks, M. Weigand, and J. Koch, ‘Dynamic Behaviour of a Rotorcraft Main Rotor System with variable speed’.
[23] *T700-401C/-701C : turboshaft engines*. One Neumann Way Cincinnati, Ohio 45215 U.S.A.: General Electrics Aviation, 2009. [Online]. Available: http://www.geaviation.com/military/engines/t700/
[24] H. Sandmaier, *Skalierung der physikalischen Gesetze und mathematischen Modellierung: Mit Anwendungen aus der Mechanik, Thermodynamik, Hydrodynamik und Elektrodynamik*. Berlin, Heidelberg: Springer Berlin Heidelberg, 2019. doi: 10.1007/978-3-662-59673-9.
[25] J. S. Nam, Y. J. Park, J. K. Kim, J. W. Han, Y. Y. Nam, and G. H. Lee, ‘Application of similarity theory to load capacity of gearboxes’, *J Mech Sci Technol*, vol. 28, no. 8, pp. 3033–3040, Aug. 2014, doi: 10.1007/s12206-014-0710-5.
[26] C. Zhang, J. Wei, S. Hou, and J. Zhang, ‘Scaling law of gear transmission system obtained from dynamic equation and finite element method’, *Mechanism and Machine Theory*, vol. 159, p. 104285, May 2021, doi: 10.1016/j.mechmachtheory.2021.104285.
[27] U. Weinberger, F. Siglmüller, J. Götz, M. Otto, and K. Stahl, ‘Scaling of planetary gear stages according to gear excitation similarity’, *Proceedings of the Institution of Mechanical Engineers, Part C: Journal of Mechanical Engineering Science*, vol. 233, no. 21–22, pp. 7246–7256, Nov. 2019, doi: 10.1177/0954406219851828.
[28] ISO, ‘ISO 6336-1 Calculation of load capacity of spur and helical gears Part 1: Basic principles, introduction and general influence factors’. 2019.
[29] ISO, ‘ISO 6336-2, Calculation of load capacity of spur and helical gears Part 2: Calculation of surface durability (pitting)’. 2019.
[30] ISO, ‘ISO 6336-3, Calculation of load capacity of spur and helical gears Part 3: Calculation of tooth bending strength’. 2019.
[31] *DIN 743-1:2012-12, Tragfähigkeitsberechnung von Wellen und Achsen_-Teil_1: Grundlagen*. doi: 10.31030/1818281.
[32] ISO, ‘ISO/TS 16281: Wälzlager - Berechnung der modifizierten nominellen Referenz-Lebensdauer für Wälzlager (ISO/TS 16281:2008 + Cor 1:2009) (konsolidierte Fassung)’. Jun. 15, 2017.
[33] ‘Home’, KISSsoft AG. Accessed: Jul. 19, 2024. [Online]. Available: https://www.kisssoft.com/en
[34] ‘CTSM242 Platform | Electric Motor | Helix UK’, Helix. Accessed: Aug. 19, 2024. [Online]. Available: https://www.ehelix.com/products/ctsm242-electric-motor/
[35] European Aviation Safety Agency, ‘Certification Specifications for Large Rotorcraft CS-29’. Dec. 2012.
[36] U.S. Department of Transportation, Federal Aviation Administration, ‘Certification of Transport Category Rotorcraft AC 29-2C’. May 2014.
[37] ‘Datenblatt HBM T40B Drehmoment-Messflansch’. [Online]. Available: https://www.hbm.com/fileadmin/mediapool/hbmdoc/technical/B03405.pdf
[38] ‘Datenblatt HBM T210 Drehmoment-Messwelle’. [Online]. Available: https://www.hbm.com/fileadmin/mediapool/hbmdoc/technical/B05814.pdf
[39] P. R. Darmstadt *et al.*, ‘Hazards Analysis and Failure Modes and Effects Criticality Analysis (FMECA) of Four Concept Vehicle Propulsion Systems’, *Vehicle Propulsion Systems*, 2019.